Estuarine, Coastal and Shelf Science 211 (2018) 238–247

Contents lists available at ScienceDirect

Estuarine, Coastal and Shelf Science

journal homepage: www.elsevier.com/locate/ecss

Assessing rehabilitation of managed mangrove ecosystems using high resolution remote sensing

Maartje Oostdijk[a,*,1], Maria J. Santos[a,b], Dennis Whigham[c], Jos Verhoeven[d], Sonia Silvestri[e,f]

[a] Copernicus Institute of Sustainable Development, Department of Innovation, Environmental and Energy Sciences, Utrecht University, The Netherlands
[b] University Research Priority Program in Global Change and Biodiversity and Department of Geography, University of Zurich, Switzerland
[c] Smithsonian Environmental Research Center, USA
[d] Ecology and Biodiversity, Department of Biology, Utrecht University, The Netherlands
[e] Nicholas School of the Environment, Duke University, USA
[f] Dep. TESAF, University of Padova, Italy

ARTICLE INFO

Keywords:
Mangroves
Impoundments
Aerial photography
Classification
WorldView-2
Mangrove LAI

ABSTRACT

Mangroves are valuable ecosystems for coastal protection, carbon sequestration and storage, and they provide habitat, refuge and rearing areas for many important marine species. To control mosquito outbreaks in coastal regions, mangroves were often impounded and managed using a variety of techniques that ranged from the application of insecticides to water level manipulation. Since continuous impounding had been shown to have negative effects on mangrove vegetation, other techniques have been used to manage hydrology in impoundments. A recent technique is called rotational impoundment management (RIM) and it involves flooding impoundments in summer and spring, the reproductive season of the mosquitos. In this study, we assessed the effects of 5 years of RIM management on mangrove vegetation in an impoundment on the east coast of Florida. We compared mangrove vegetation in the RIM impoundment with an adjacent impoundment that was not managed. We created a map of leaf area index (LAI) to assess vegetation productivity and its change in the two impoundments. We classified color-infrared aerial photographs from 2008 to 2010 and a WorldView-2 satellite image from 2014 to measure the extent of mangrove vegetation types and temporal changes in the two impoundments. We found a 38% increase in cover of dense mangrove vegetation after five years for the RIM-impounded area. Classification accuracy was around 80% for all imagery. The increased growth of plants and cover of dense mangroves in the RIM impoundment was corroborated by observed leaf area index values. Overall, the study demonstrates that vegetation in the RIM impoundment is becoming denser and in the near future will probably become similar to an impoundment that is open to tidal exchange or mangrove dominated areas that are not impounded.

1. Introduction

Mangroves are important ecosystems for coastal protection, carbon sequestration (Chmura et al., 2003) and storage (Donato et al., 2011), and are used as a key habitat component by many marine species (Tomlinson, 1986; Alongi, 2008; Barbier and Hacker, 2011, Doughty et al., 2017). Mangrove trees stabilize shorelines by developing root systems that reduce erosion and collectively coastal mangroves are "bio-shields" against destructive impacts from storms or storm surges (Tomlinson, 1986; Alongi 2008). Approximately 75% of the world's mangroves occur in 15 countries, and only 6.9% are protected under the existing protected areas network (IUCN protected areas categories I–VI) (Giri et al., 2011). While the benefits of mangrove dominated ecosystems are widely appreciated, the extent of mangroves has diminished worldwide due to clear felling for urban development and destruction of habitat for fish and invertebrate aquaculture (Duke et al., 1998; Alongi, 2002; Vogt et al., 2012; Feller et al., 2017). Moreover, management strategies for mangrove dominated wetlands can have damaging effects on vegetation and water quality (Jimenez et al., 1985; Rey et al., 1990; Hatton and Couto, 1992; Rey et al., 2012; Verhoeven et al., 2014). Impounding mangroves, for example, has been a traditional management strategy that has been used to control mosquito populations, however this technique resulted in extensive die-back of mangrove vegetation (Rey et al., 1990, 2012; Verhoeven et al., 2014). Recently, rotational impoundment management (RIM) of previously impounded mangroves has been proposed as an alternative solution to

* Corresponding author.
E-mail addresses: maartje.oostdijk@gmail.com, mtn1@hi.is (M. Oostdijk).
[1] Present/permanent address: Askja 270, Reykjavik, 101 Iceland

https://doi.org/10.1016/j.ecss.2018.06.020
Received 15 January 2017; Received in revised form 5 June 2018; Accepted 18 June 2018
Available online 20 June 2018
0272-7714/

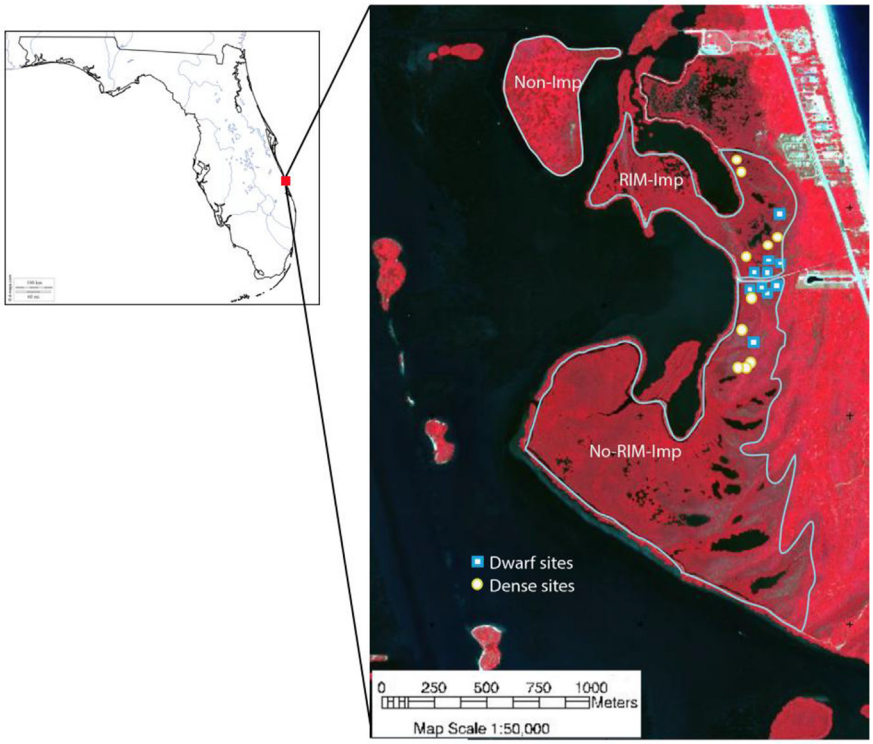

Fig. 1. Study area locations in Florida, United States and location of the sites selected for the analysis on a color-infrared composite using WV-2 data (Band 7 Red, Band 5 Green, Band 3 Blue). (For interpretation of the references to color in this figure legend, the reader is referred to the Web version of this article.)

management of hydrologic conditions that results in effective management of noxious insects while benefiting mangrove vegetation. The long- and short-term benefits of RIM on mangrove vegetation, however, have not been quantified.

Impoundments of wetlands in the Indian River Lagoon, Florida, were constructed between the late 1950s and 1960's for purposes of mosquito control. The common black salt marsh mosquito (*Aedes taeniorhynchus*) does not oviposit in standing water (Rey et al., 2012), therefore the impoundments were expected to decrease mosquito populations. Artificial dikes were built around the wetland that were known to be source areas for mosquitos and they were initially kept permanently flooded (Rey et al., 2012). The consequences of eliminating tidal exchange between impoundments and the adjacent estuary were negative for vegetation, fish communities and water quality (Brockmeyer et al., 1996). Halophyte species such as saltwort (*Batis maritima*), glasswort (*Salicornia virginica*) and dwarf glasswort (*Salicornia bigelowii*) disappeared inside the impoundments. Red mangrove (*Rhizophora mangle*) was the only plant species that benefitted from impounding water as it can better withstand submersion (Rey et al., 1990). Since the early 1960's there have been efforts to rehabilitate the impoundments by hydrologically reconnecting them to the adjacent estuary that, in eastern Florida, is primarily the Indian River Lagoon (Brockmeyer et al., 1996; Bosire et al. 2008; Rey et al., 2012). The most recent approach to management of impoundment hydrology is RIM (Rey et al., 2012). RIM involves pumping estuarine water into the impoundment between March and September, during which time the culverts that connect the impoundment to the estuary are closed. RIM results in raising the water level in the impoundment by 30 cm. The management objective is to flood the impoundments during the mosquito reproductive season (spring and summer) to reduce their reproductive output (Verhoeven et al., 2014). RIM has been found to result in changes in the nutrient dynamics of black mangrove (*Avicennia germinans*) mangroves that are present in the impoundments. The nitrogen content of leaves is increased as is the rate of growth of mangrove shoots; including higher rates of leaf production of black mangrove (Verhoeven et al., 2014). RIM also resulted in a 43% decrease in the salinity of interstitial water in the impoundments (Laanbroek et al., 2012). Despite the results now available through observations in specific study sites, research on the response of mangroves to RIM at the scale of an entire impoundment are still missing.

Spatial and spectral characteristics of mangrove vegetation have been used to indicate changes in leaf area index (LAI), biomass and photosynthetic activity (Green et al., 1998; Kuenzer et al., 2011). In general, satellite and airborne remote sensing has been successfully applied to track the condition of vegetation in mangroves and salt-marshes (Belluco et al., 2006; Rey et al., 2009). High spatial resolution satellite imagery from WorldView-2 and GeoEye-1 have been used to assess mangrove productivity (Heumann, 2011; Pu and Cheng, 2015), to discriminate species and estimate biomass, and assess related vegetation function and morphology (Kovacs et al., 2009; Heenkenda et al., 2014). Remote sensing imagery has also been used to detect changes in mangrove ecosystems (Lee and Yeh, 2009). Aerial photographs have also been used to classify and map mangrove forests and assess changes in coastal ecosystems (Geneletti and Gorte, 2003; Krause et al., 2004; Kuenzer et al., 2011).

In this study we examined changes in the density of black mangrove (*Avicennia germinans*) under differing hydrologic conditions. We used high spatial resolution aerial photographs (0.15 m and 0.3 m) and World View-2 satellite imagery (2 m) to quantify changes in black mangrove in an impoundment in which RIM was employed. For comparisons we examined mangroves in an adjacent impoundment (Non-RIM) that was open to tidal change, and a third mangrove-dominated area (i.e., Non-Imp, control) that never was impounded.

2. Methodology

2.1. Study area

The two impoundments are located on the east side of the Indian River Lagoon between Vero Beach and Fort Pierce, Florida (Fig. 1). The

levee surrounding the impoundment area that is open to tidal exchange (No-RIM-Imp; Fig. 1) was breached in 1979 and water levels are since then largely been controlled by tidal circulation (Verhoeven et al., 2014). RIM management was started in the other impoundment (RIM-Imp; Fig. 1) in March 2009. It is annually flooded between March and September by pumping water into it from the Indian River Lagoon and water levels of 30 cm are maintained during the approximately seven month management period (Verhoeven et al., 2014). During the other months, the impoundment is subjected to tidal exchange through a series of tide gates.

In addition to the remote sensing data, in March 2015 we collected vegetation and LAI data from 20 plots (Fig. 1, sites originally described in Verhoeven et al., 2014) distributed over the two impoundments (RIM-Imp and Non-RIM-Imp, 10 plots in each) and covering two mangrove types: dwarf and dense. In each impoundment, dwarf mangrove corresponded to 30% or less canopy cover, where the tree canopies were not in contact and the trees were ≤1 m high; five plots were set in this vegetation type. Five plots were set in dense mangrove with 80% or more canopy cover and the trees were taller than 3 m. Originally, we collected data on a third mangrove type, a sparse category. However, as a follow up of previous studies (Verhoeven et al. 2014) we expected that mangroves would experience enhanced growth in response to the altered hydrology of the impoundments. We thus expected improved growth under RIM overtime, with dwarf plants increasing in size and leaf area and becoming sparse, and sparse plants would enter the dense category. Thus, for classification purposes we did not use the sparse category because this category was the most dynamic and therefore more prone to error, and classified mangroves as either dwarf or dense. The choice of cover types was based on the typical zonation of mangrove vegetation inside impoundments (Feller et al., 2003). Dwarf mangrove zones are typically located in the interior of the impoundments where salt pans, areas devoid of vegetation except for patches of saltwort (*Batis maritima*) or Virginia glasswort (*Salicornia* spp.), also occur due to high levels of evaporation and isolation from tidal circulation. Black mangrove is dominant where salinity values approach those of seawater, as black mangrove tolerates high salinity conditions better than red mangrove (*Rhizophora mangle*). Red mangrove is denser in areas of the impoundments that are continuously flooded, such as the waterways that are at the border of the impoundments and the lagoon and the non-impounded mangrove, as shown in Fig 1 (Feller et al., 2003).

2.2. Data collection and pre-processing

2.2.1. Remote sensing data

We used WorldView-2 (WV2) satellite data and airborne aerial photographs (Table 1). WV2 data were collected on June 2014. Airborne aerial photographs were provided by the Florida Department Of Transportation and include two datasets, one collected in April 2008 with a Digital Mapping camera (DM, Intergraph) and the second collected in December 2010 with a UltracamX camera (UCX, Vexcel).

2.2.2. Field data

Field sampling occurred during the first two weeks of March 2015. At the time of field sampling the mangroves were not yet inundated.

2.2.2.1. Reflectance data at pseudo-invariant targets. These data were collected for the radiometric calibration of the aerial photographs and panchromatic band of the WV2 image. Since there was no ground truth reflectance data available at the time of image collection, we chose targets for which reflectance values are not expected to change over time, i.e., invariant targets (Hadjimitsis et al., 2009). We chose at least four dark and bright targets that were present in each aerial photograph (e.g., marina, gravel road, water surface, dark and light asphalt). We collected field reflectance of pseudo-invariant targets across the three mangrove areas using an ASD Fieldspec Pro spectro-radiometer (ASD Inc, 2002) that collects reflectance data over 350–2500 nm with a spectral resolution of 3–5 nm in the VNIR range. We used a white reference panel to calibrate the ASD in between measurements. For each target we averaged five measurements of the field spectrometer to retrieve the reference spectra.

Table 1
Location, spatial resolution, collection date and spectral resolution of the images from Digital Mapping camera (Intergraph, 2009), UltracamX (Christopherson, 2010) and WV2 (Updike and Comp, 2010).

Sensor	Satellite: WV2 multispectral	Airborne: UltracamX	Airborne: Digital Mapping camera
Study sites	RIM-Imp, no-RIM-Imp, Non-Imp	RIM-Imp, no-RIM-Imp, Non-Imp	RIM-Imp, Non-Imp
Collection date	10-June-2014	03-December-2010	22-April-2008
Spatial resolution	2 m	0.15 m	0.30 m
Spectral bands (nm)			
Blue coastal	400–450		
Blue	450–510	410–540	400–580
Green	510–580	490–660	500–650
Yellow	585–625		
Red	630–690	590–700	590–675
Red Edge	705–745	690–980	675–850
NIR1	770–895		
NIR2	860–1040		
Panchromatic (0.5 m)	450–800		

2.2.2.2. Leaf area index. We collected *in situ* LAI measurements at 161 locations (in the plots and elsewhere) within the RIM and no-RIM impoundments dominated by dwarf and dense mangroves. We did not collect LAI measurements in the Non-Imp area due to the limited time we had in the field. Data was collected on 10 sunny days during the first two weeks of March, between 10AM and 2PM. We used a portable AccuPAR LP-80 (Decagon Devices), which measures incoming radiation in the photosynthetic range (400–700 nm) and has been shown to give accurate estimates of LAI (Facchi et al., 2012; Wilhelm et al., 2000). For densely vegetated areas a Photosynthetic Active Radiation (PAR) meter and data logger were installed on the dike of the impoundment. The data logger recorded one measure of PAR every 30 s above the canopy. For each above canopy PAR measurement, we averaged 10 below canopy PAR measurements, taken in a circle from a central position (Kovacs et al., 2009), as measurement of below canopy PAR is more prone to noise due to scattering within the canopy. This methodology allows a more reliable estimate of average light levels that pass through the canopy as there is large variability in light levels (Decagon Devices). We matched the timestamps of the PAR measurements of the data logger and AccuPAR and post-processed the data in a spreadsheet provided by Decagon Devices to calculate LAI values.

2.2.2.3. Vegetation type. In each of the plots that were sampled, we recorded locations of individual mangrove trees and mangrove associated species (N = 214) using a GPS device (Garmin GPSMap 78) with 2 m positional accuracy. Because of the 2 m accuracy of the GPS device, we selected plots in relatively homogeneous areas larger than 2 × 2 m, with the exception of dwarf trees that were single trees visually identified in the high-resolution imagery. We recorded information on the black mangrove classes that were present, as well as mangrove associate species like saltwort and Virginia glasswort.

2.2.3. Pre-processing of remote sensing data

2.2.3.1. Georeferencing. The aerial photographs (DM and UCX) were orthorectified by the provider (Aerial Cartographics of America, Orlando, Florida) (Humphrey, 2011). We georeferenced the WV2 multispectral and panchromatic bands using image to image

Table 2
Selected vegetation indices to regress against *in situ* LAI measurements (for the wavelengths of the bands used see Table 1).

Vegetation index	Formula
Normalized difference vegetation index 1 (NDVI1)	$\frac{\rho_{NIR1}-\rho_{RED}}{\rho_{NIR1}+\rho_{RED}}$
Normalized difference vegetation index (NDVI $_{(bands\ 7\&6,\ 5\&4)}$)	$\frac{\left(\frac{\rho_{REDEDGE}+NIR1}{2}\right)-\left(\frac{\rho_{YELLOW}+\rho_{RED}}{2}\right)}{\left(\frac{\rho_{REDEDGE}+NIR1}{2}\right)+\left(\frac{\rho_{YELLOW}+\rho_{RED}}{2}\right)}$
Simple Ratio 1 (SR1)	ρ_{NIR1}/ρ_{RED}
Simple Ratio (SR $_{(bands\ 7\&6,\ 5\&4)}$)	$\left(\frac{\rho_{REDEDGE}+NIR1}{2}\right)/\left(\frac{\rho_{YELLOW}+\rho_{RED}}{2}\right)$
Modified Soil Adjusted Vegetation Index (MSAVI 2)	$\frac{2\rho_{NIR1}+1-\sqrt{(2\rho_{NIR1}+1)^2-8(\rho_{NIR1}-\rho_{RED})}}{2}$
Modified Soil Adjusted Vegetation Index (MSAVI 2$_{(bands\ 7\&6,\ 5\&4)}$))	$\frac{\rho_{REDEDGE}+NIR1+1-\sqrt{(\rho_{REDEDGE}+NIR1+1)^2-8\left(\left(\frac{\rho_{REDEDGE}+NIR1}{2}\right)-\left(\frac{\rho_{YELLOW}+\rho_{RED}}{2}\right)\right)}}{2}$

registration in ENVI 4.7 software (Exelis Inc, Virginia, USA), using the 2010 aerial photographs as a base image and selecting 21 ground control points. The procedure achieved a sub-pixel spatial accuracy for all the multispectral bands (RMSE = 0.37 pixels), and for the panchromatic band (RMSE = 0.5 pixel). Image-to-image registration was also used to co-register the 2008 aerial photographs using the 2010 image as the base image, with a final RMSE of 0.42 pixel.

2.2.3.2. Atmospheric and radiometric correction. The aerial photographs used in this study contain 8-bit digital numbers stretched by the provider to supply a good visualization of the product. To rescale the data and convert the values to reflectance, we followed two steps. First, we performed a dark pixel subtraction in ENVI 4.7 to correct for the additive minimum signal that is caused by scattering particles and illumination differences (Heenkenda et al., 2014). In the second step we used the reflectance data of the field pseudo-invariant targets to convert the digital numbers of the aerial photographs (2008 and 2010) to reflectance values (Honkavaara et al., 2009). The conversion was done assuming that the reflectance of the selected targets was barely or not affected by radiometric changes between the date of the flights and the field campaign in March 2015. To obtain an empirical line (Pu and Landry, 2012) we built linear regressions between field reflectance and aerial photograph digital numbers of the corresponding pixels and applied the regression equations to all the other pixels.

To convert the digital numbers of the WV2 image to at-sensor radiances, we used the gain values found in the metadata. The atmospheric correction was performed using FLAASH that runs the MODTRAN5 radiative transfer model (Manakos et al., 2011). The WV2 panchromatic band was atmospherically corrected using the same empirical line method as above. See Appendix A1 in the supplementary material for a detailed explanation of the radiometric correction and the equation used.

2.2.3.3. Pan-sharpening. We created a pan-sharpened WV2 image to obtain a higher spatial resolution (Heenkenda et al., 2014; Pu and Landry, 2012). We fused the 2 m resolution multispectral bands with the 0.5 m resolution panchromatic band using the Gram-Schmidt (GS) algorithm, which has been shown to give high performances especially in forested areas (Padwick et al., 2010). This algorithm involves a several-step process and uses the spectral response curve for the given sensor (the spectral response curve for WV2 can be found in Updike and Comp, 2010) and a simulated panchromatic band from the lower spatial resolution multispectral bands (Laben and Brower, 2000). Pan-sharpening can result in spectral distortions (Laben and Brower, 2000), and to test for these effects we established classifications with the pansharpened and the 2-m WV2 image. As the difference in accuracy was small we chose the sharpest image for further change detection analyses.

2.3. Data analysis

The *in situ* LAI measurements were used to infer the spatial variation of the canopy density across the study sites, as LAI has been found to be good metric for canopy density (Machado and Reich, 1999). Moreover, several examples of the high correlation of LAI with a number of Vegetation Indexes (VI) in general (Zhao et al., 2007; Pu and Cheng, 2015) and specifically in mangrove systems (Green et al., 1998; Vega-Rodríguez, 2008) have been demonstrated. Here we investigated the correlation between our LAI measurements and a set of VIs (Kovacs et al., 2009; Pu and Cheng, 2015) calculated using the 2014 WV2 dataset (which was collected a few months before the field survey). This method allowed us to determine the index that correlates best with LAI and choose it for mapping LAI in the study areas and use it for classification purposes.

We first matched *in situ* LAI coordinates with the coordinates of the georeferenced and atmospherically corrected WV2 image in ENVI 4.7 software. Then we selected a pool of indexes that showed a significant correlation with LAI in previous studies of mangrove forests (Kovacs et al., 2005; Kovacs et al., 2009; Table 2). We also added the Modified Soil Adjusted Vegetation Index (MSAVI2), as this index is known to correct for the signal caused by bare soil in sparsely vegetated areas, and we expected it to perform better for our dwarf mangrove sites (Qi et al., 1994). To find out if the differences we observe in the vegetation index are related to *in situ* changes in canopy density, we correlated the field observed changes with the remote sensing vegetation index.

The different VIs used in our approach were calculated using raw and modified WV2 red and NIR bands. WV2 spectral bands have narrower bandwidths than the aerial photographs (Table 1), therefore a direct comparison may result incorrect. We combined some of the WV2 bands in order to match the bands of the aerial photo cameras. This approach requires to know a priori the spectral response curves of the aerial photographs in order to correctly weight the signal (Heenkenda et al., 2014). Unfortunately, the spectral response curves of the two cameras were not available, so we assigned a response equal to 100% to all the bands used in the process. Specifically, the modified red band was created by averaging the reflectance of the red and yellow bands of the WV2 image because both bands spectrally overlap with the red band of the aerial photographs (Table 1). Using the same approach, we created a modified NIR band by averaging the reflectance of the red-edge and NIR1 band of the WV2 image because both bands overlap with the NIR of the aerial photographs (Table 1). We then regressed LAI against all vegetation indices listed in Table 2, and the regression model that achieved the highest R-squared was selected to produce a LAI map for the entire study area.

To understand whether mangrove vegetation density changed over time, we developed a classification method based on a range of values of the selected VI calculated with the 2008 and 2010 aerial photographs and the 2014 WV2 satellite image. Similar classification methods based

on VI´s ranges have been used in previous studies (Kovacs et al., 2005a; Lee and Yeh, 2009; Lehmann et al., 2015), achieving high classification accuracy. To more accurately represent temporal changes over the time period covered by the aerial photographs and at the impoundment scale, our classification method aimed at classifying two (dwarf and dense) mangrove classes as well as bare soil and herbaceous vegetation. We used the field location data to delimit the dwarf and dense vegetation sites (Fig. 1) and to detect areas with bare soil (i.e., pans) and areas with only herbaceous vegetation. We used the field locations to define Regions of Interest (ROIs) within the WV2 image. For the aerial photographs, since these were collected a few years before the field campaign (in 2008 and 2010), we chose ROIs based on visual inspection of tree crown dimensions (Rodriguez and Feller, 2004). Table A1 in the supplementary material shows the number of ROIs that were used for each cover class for each year and imagery type. ROIs have an area of at least 2 × 2m (4 m^2) and include a minimum of one pixel in the original WV2 image, approximately 16 pixels from the pansharpened image, and 44 (22-April-2008) and 177 (03-December-2010) pixels in the aerial photographs.

We divided the ROIs into training and testing sets for model development and assessing the accuracy of the classification (Table 2). We calculated the mean and standard deviation of the VI values for each cover class using the training ROIs. This was to establish the VI confidence interval (mean ± standard deviation) per class, and this confidence interval was used across each image to classify each mangrove cover class. To ensure that the confidence intervals corresponded to separable cover classes, we used ANOVA to test for significant differences among classes at a significance level of $p < 0.01$. We used this strict significance level because of several problems related to VI measurements, such as scattering of soil and vegetation in lower values (Gonsamo and Pellikka, 2012). We tested the VI data for homogeneity of variance and because of the unequal sample sizes we used the harmonic mean in the ANOVA. We then assessed the accuracy of our results using the validation ROIs. We created a confusion matrix for each imagery type, and calculated the percent correct classification rate, kappa statistics, and user's and producer's accuracy (Landis and Koch, 1977; Congalton, 1991).

We used the classification map to measure the percent cover of dwarf and dense mangrove classes. We used change detection to assess whether there were differences among the treatment (RIM and continuous impoundment) and control (non-impounded) mangrove areas. Since we did not have imagery over the No-RIM-Imp in 2008, we calculated the percent cover for years 2008, 2010 and 2014 in RIM-Imp and Non-Imp, and for years 2010 and 2014 in No-RIM-Imp areas. We finally calculated a post-classification transition matrix to assess changes from 2008 to 2010, and from 2010 to 2014.

3. Results

3.1. Leaf area index of mangroves

This analysis aims at studying the possible correlation between the LAI values measured in the field and the different indices that can be retrieve from WV2. The mean LAI for the field sites was 2.6. Dense mangrove sites had higher LAI values (mean LAI = 3.64) than dwarf sites (mean LAI = 1.33) (see Fig. 2).

All the linear regression models between LAI and the vegetation indices fitted the data quite well, and R^2 values were high suggesting strong explanatory power (Fig. 3). The $SR_{(bands\ 4\&5,6\&7)}$ shows the strongest correlation with LAI ($R^2 = 0.7067$; F = 346.9, P-value < 0.001). MSAVI2 and all the NDVIs showed a strong linear correlation with field LAI, however, visual inspection of the scatter plots suggests that at LAI > 4 and LAI < 1.5 the relationship becomes non-linear. This pattern was less strong for the simple ratios (Fig. 3), hence $SR_{(bands\ 4\&5,6\&7)}$ was used as the selected metric to perform the classification of the WV2 image.

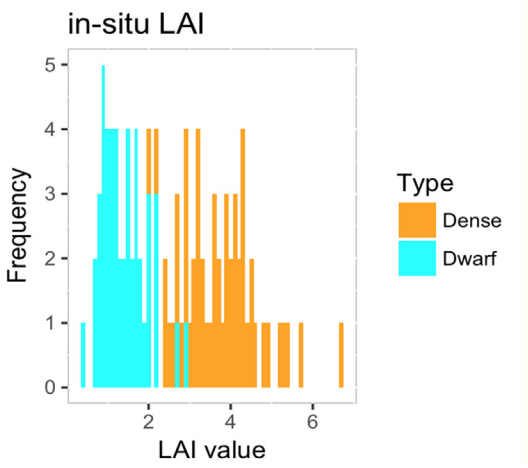

Fig. 2. Histogram of *in situ* LAI recordings in dense and dwarf field sites collected on 10-06-2014.

From the LAI map it can be seen that both impoundments have a similar percentage cover of denser LAI values and a clear mangrove vegetation zonation can be seen (Fig. 4). Vegetation in the impoundments becomes sparser land-inward, where larger areas with dwarf and herbaceous vegetation are found. The higher LAI vegetation that can be seen eastward of the sparser mangrove area is the upland forest (pink line in Fig. 4b). The control area had higher LAI than both impounded areas (mean LAI = 4.58), and the RIM-Imp showed the lowest average LAI (mean LAI = 3.38); the No-RIM-Imp had intermediate LAI (mean LAI = 3.44).

3.2. Land cover classification and change detection

On the basis of the results described above, SR was used to map mangrove land cover for the aerial photographs and $SR_{(bands\ 4\&5,\ 6\&7)}$ was used for WV2. Mangrove cover classes SR values were significantly different in 2008, 2010 and 2014 (Fig. 1 and Table C1). SR values ranged from 1.33 to 10. Means, standard deviations and the established ranges of SR values for all vegetation classes for 2008, 2010 and 2014 can be found in Table C1, the details of the ANOVA results can be found in the supplementary material (Table C2).

Fig. 5a, 5b and 5c show the normalized frequency distribution of the SR pixel values of the four classes retrieved with the classification for the three dates (2008, 2010 and 2014 respectively). We notice that the distribution of both dwarf and dense vegetation migrates overtime from lower to higher SR values, suggesting that the density cover has increased. Looking at the maps (Fig. 5d, 5e and 5f) we see a transition from dwarf mangrove towards more dense mangrove from 2010 to 2014 with larger presence of dwarf vegetation further away from the estuary (cyan in Figure 4). The maps clearly show that the Non-Imp area has a denser cover of mangrove vegetation (orange) than the RIM-Imp in all time steps. This is confirmed by the percentage coverages reported in Fig. 6, where it can be observed that the RIM-Imp areas were mostly covered by a mix of dense and dwarf vegetation in 2008 whereas the non-impounded areas had mostly dense vegetation. In 2010 RIM-Imp showed a greater area covered with dense vegetation, similar to that of No-RIM-Imp. Finally, by 2014 RIM-Imp achieved a high percentage cover of dense mangrove with dwarf mangrove patches (Fig. 6).

Dense mangrove and soil classes achieved the highest accuracies in all the images, while dwarf mangrove and herbaceous classes had the lowest accuracies. Accuracy was slightly higher for the aerial photographs (84–86%) than for the WV2 image (78%). Overall, the accuracy obtained for the 2008 aerial photographs was higher than for the 2010 aerial photographs, mainly due to lower accuracies in the dwarf and

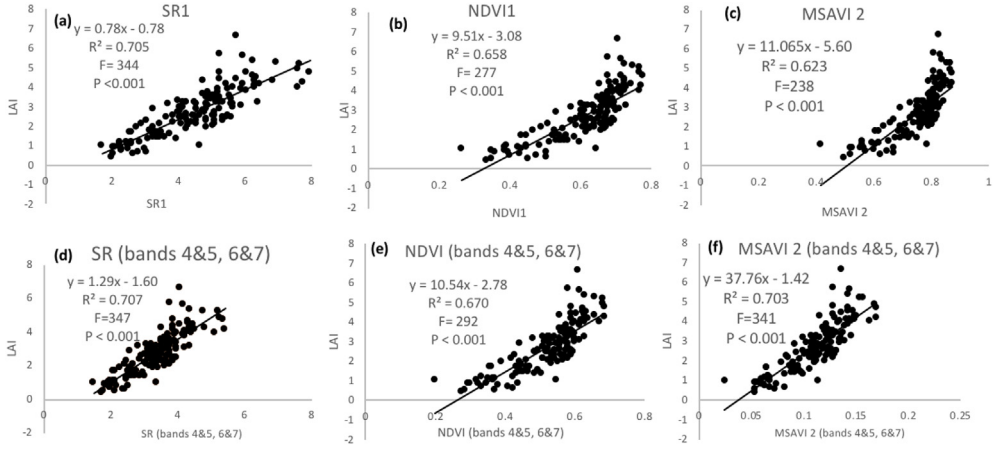

Fig. 3. Regression of LAI and vegetation indices using different combinations of WV bands: a) SR1 b) NDVI1 c) MSAVI 2 d) $SR_{(bands\ 4\&5,\ 6\&7)}$ e) NDVI $_{(bands\ 4\&5,\ 6\&7)}$ f) MSAVI 2 $_{(bands\ 4\&5,\ 6\&7)}$.

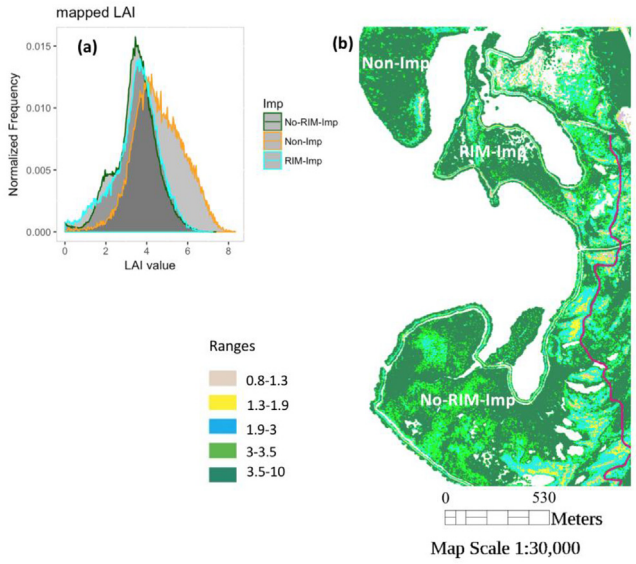

Fig. 4. a) Histogram of distribution of the LAI values across the study areas (2 m WV-2, 2014). Colors indicate the three different areas: No-RIM-Imp, Non-Imp, and the RIM-Imp. b) distribution of the LAI values across the field campaign sitemap on 10-06-2014. Colors indicate ranges of LAI. This map was produced with $SR_{(bands\ 4\&5,6\&7)}$. It can be observed that both impoundments have a gradient of LAI of mangrove vegetation from lower to higher, with the lowest LAI vegetation found in the interior of the impoundment. (For interpretation of the references to color in this figure legend, the reader is referred to the Web version of this article.)

herbaceous classes (Table 3).

Based on the final maps (Fig. 5), we calculate that in 2010, 59% of the RIM-Imp area was covered by dense mangrove, a lower value than the 79% in the No-RIM-Imp and the 90% of the No-Imp area. In 2014, the dense mangrove in the RIM-Imp area increased to 74%, a value similar to that in the No-RIM-Imp area. We found a relatively stable vegetation cover in the Non-Imp area over time, mostly of dense mangrove (Fig. 6). Between 2008 and 2010, the dense mangrove area in the RIM-Imp increased by 47,939 m^2 (Table 4, +7% of the area) and 52,434 m^2 (Table 4, +8% of the area) over 2010–2014. Unfortunately the No-RIM-Imp was not captured in the 2008 survey; however, comparing 2010 and 2014 we found that dwarf vegetation was replaced by dense vegetation around 4% of the area (Figs. 5 and 6). In the No-RIM-Imp area there was no overall increase in the dense vegetation class.

In all three years, dwarf and dense mangrove vegetation had the largest percent cover inside the impounded areas, while the Non-Imp control area was mainly covered by dense mangrove vegetation (Fig. 6). In all three areas, only a low percentage of the sites had bare soil or areas covered by a few scattered dwarf black mangroves and herbaceous vegetation (Fig. 5), with small between year fluctations (Table 4). Areas covered by soil, herbaceous vegetation and dwarf mangrove vegetation in the RIM impoundment were recolonized by mangrove trees (Fig. 5 and Fig. F1 in supplementary material show details from the CIR imagery from the interior of the RIM impoundment 2008–2010).

4. Discussion

Our results show how RIM has promoted succession towards denser mangrove vegetation, probably linked to RIM-induced changes in salinity and freshwater availability. This could be because as RIM causes salinity levels to decrease it promotes an environment more suitable for mangrove to establish and persist. The observed changes were likely explained by the fact that plant community composition in mangroves is mainly controlled by salinity (Stringer et al., 2010). Black mangroves tolerate high salinity conditions by actively excreting salt from the leaves but, as suggested by Atkinson et al. (1967), this active process requires energy from the mangroves, thus also limiting growth of these species under very high salinity conditions. Moreover, salinity induced stress increases demand for nitrogen, a nutrient that had been shown to limit mangrove growth in the non-RIM impoundment (Feller et al., 2003). The implementation of RIM resulted in a significant reduction in the salinity of interstitial water and an increase in the levels of plant extractable nitrogen in black mangrove leaves (Verhoeven et al., 2014), both factors were probably related to the changes in cover that we observed at dwarf sites using aerial imagery. Moreover, less dwarf and herbaceous vegetation was found in the non-impounded areas, again suggesting that the hypersaline conditions are a characteristic of impounded mangrove areas affecting mangrove vegetation performance (Feller et al., 2003).

The LAI map shows a gradient of sparser to dense cover in the impounded areas. In these sites denser mangrove vegetation was located on the side of the lagoon while land-inward mangrove vegetation became sparser which is in agreement with the zonation described by Feller et al. (2003). We found a mean *in situ* LAI of 2.6, which approximates the values found for dwarf stands (Kovacs et al., 2009). The average LAI recorded for the dense vegetation corresponds to the higher range of the abovementioned values for black mangrove LAI (Ramsey and Jensen, 1996; Kovacs et al., 2005b, 2009).

In 2010 the No-RIM-Imp still shows a denser cover of mangrove than the RIM-Imp, while in June 2014 the cover types were similar in both impoundments. We observed shifts in vegetation cover in the RIM-

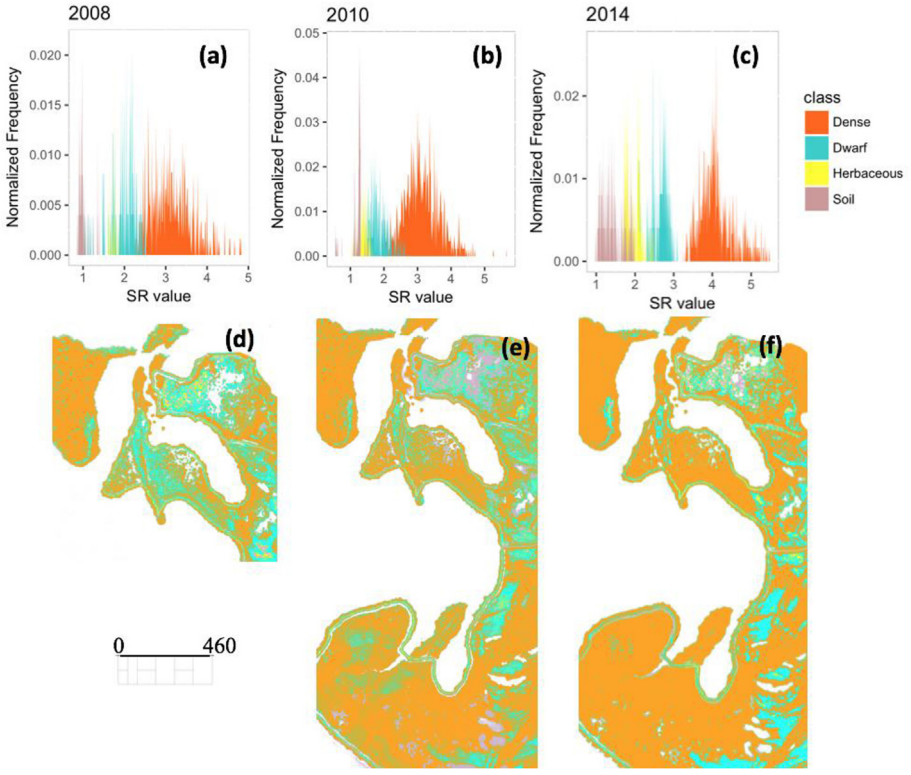

Fig. 5. Histograms of SR values for the different vegetation classes in: (a) 22-04-2008; (b) 03-12-2010; and (c) 10-06-2014. Land cover and classification results for the study area in (d) 2008 (aerial photograph), (e) 2010 (aerial photograph), (f) 2014 (0.5 m WV-2, pan-sharpened image).

Imp but also in our control areas. These changes can't be accounted for by the management implementation only and likely also interfere with our quantification of the shifts in landcover in the RIM-Imp. There are several reasons that could account for the observed shifts in vegetation. The shift towards denser vegetation in the No-RIM-Imp area between 2010 and 2014 could be due to spillover effects from the RIM implementation, because this area is in close proximity to the No-RIM-Imp area and especially in the northern part the inundation of the RIM-imp also causes parts of the No-RIM-Imp to be submerged. The increase in dense vegetation in the RIM-Imp was however always stronger than in the control areas, suggesting a positive effect of the RIM management on the rehabilitating mangrove area.

Even though we observed a shift toward denser mangrove vegetation in the RIM impoundment, the cover of dense vegetation was higher in the non-RIM impoundment and the control area. This suggests that even though there had been significant changes in the RIM impoundment, they had not yet resulted in differences that mirrored vegetation in the other two sites sampled. The non-RIM impoundment does not seem to exhibit an increase in dense vegetation, the non-impounded area does have a small increase in the dense vegetation class (89% dense mangrove vegetation in 2010 and 92% dense mangrove vegetation in 2014). The non-RIM impoundment and the control area had more red mangrove compared to the RIM impoundment, thus RIM management has begun to cause changes in the vegetation that will only fully be accounted for over time. Red mangrove is more tolerant of flooding (Rey et al., 2009) and during our field campaign one of us (DW) noted that red mangrove seedlings and saplings were more common in the three vegetation types dominated by black mangrove than they had been in the early 2000s (DW). Given that the red mangroves were still small, however, the increase in canopy cover that was observed in the RIM impoundment was more likely due to increased canopy density and increased productivity of black mangrove. RIM was introduced in March 2009, so about 11 months after the picture from 2008 to 17 months before picture from 2010 to 41 months before the picture of 2014. We would have expected a greater shift between 2010 and 2014 than between 2008 and 2010 as there would have been more time for the dense mangrove vegetation to restore. One reason for the absence of such a pattern could be that the addition of estuarine water

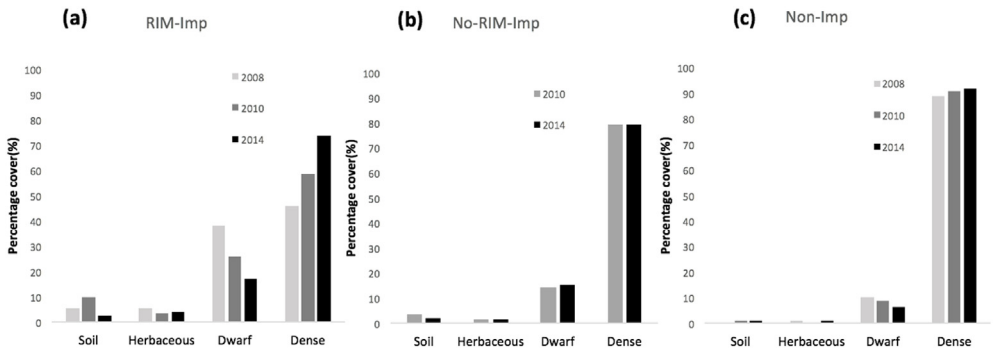

Fig. 6. Percent cover (%) of soil and vegetation density classes for the three mangrove areas: (a) RIM-Imp; (b) No-RIM-Imp and (c) Non-Imp.

Table 3
Overall accuracy, kappa coefficient and user's and producer's accuracy for the different density classes for 2008 and 2010 (aerial photographs) and 2014 (WV2) both for the pan-sharpened (0.5 m) and the non-pansharpened (2 m) products.

Year	Image	Overall accuracy (%)	Kappa coefficient	Accuracy (%)	soil	herb	dwarf	dense
2008	DM	86%	0.799	Producer's	100	51	77	97
				User's	98	69	67	96
2010	UCX	84%	0.84	Producer's	95	43	88	100
				User's	78	75	84	93
2014	WV2_05 m	78%	0.69	Producer's	69	57	80	100
				User's	97	77	52	98
	WV2_2 m	78%	0.66	Producer's	80	46	56	95
				User's	74	31	70	97

Table 4
Change detection matrix (m^2) to assess the landcover change between the years before and after implementing RIM.

Year/Area	Class	Soil	Herbaceous	Dwarf	Dense	Class Total
2008/ 2010 RIM-Imp	Soil	13592	4406	5486	1401	24885
	Herbaceous	2699	3273	5946	1469	13388
	Dwarf	5146	9154	45999	24096	84395
	Dense	1349	3880	69667	163856	238753
	Class Total	22786	20713	127099	190822	
	Image Difference	2099	−7325	−42704	47931	
2010/ 2014 RIM-Imp	Soil	6116	584	1232	492	8424
	Herbaceous	6909	2808	4833	1915	16464
	Dwarf	11788	7326	33970	23050	76133
	Dense	9853	5326	62711	202643	280533
	Class Total	34666	16044	102745	228098	
	Image Difference	−26242	421	−26613	52434	
2010/ 2014 No-RIM-Imp	Soil	5789	547	2144	5639	14118
	Herbaceous	3049	1152	4368	5109	13678
	Dwarf	8888	7146	52917	61535	130486
	Dense	17094	5616	81133	605299	709141
	Class Total	34819	14461	140562	677582	
	Image Difference	−20701	−783	−10076	31560	
2008/ 2010 Non-Imp	Soil	1906	528	750	127	3311
	Herbaceous	174	243	480	125	1022
	Dwarf	552	905	4585	5603	11646
	Dense	244	821	14179	126087	141332
	Class Total	2877	2498	19995	131941	
	Image Difference	435	−1476	−8349	9391	
2010/ 2014 Non-Imp	Soil	524	61	321	784	1689
	Herbaceous	374	48	262	871	1554
	Dwarf	819	256	2464	6395	9933
	Dense	1566	680	11121	126665	140031
	Class Total	3282	1046	14167	134714	
	Image Difference	−1593	509	−4234	5317	

to the impoundment resulted in a rapid change in the soil salinity pattern within the impoundment (a decrease in the dwarf and sparse areas) resulting in a rapid vegetation response that continued, but at a slower rate, in subsequent years.

Our SR-based classification was successful, with high overall classification accuracy. However, during the study we experienced several conditions that could have affected SR and therefore classification accuracy. First, despite the ANOVA results (Table C2) that show us that all our classes are significantly different at the $p < 0.001$ level, we obtain rather low accuracy for our low-density classes, as can be seen in Fig. 5a there is substantial overlap between the herbaceous and dwarf class. We put more emphasis on the shifts in the mangrove vegetation classes, especially for the years 2008 and 2010. Second, at the time of the collection of the WV2 image (June 2014) the dwarf sites were flooded and the standing water that was present could have resulted in SR that would be different if the areas had not been flooded. Third, other studies show that it is possible to move beyond vegetation indices and were able to distinguish mangroves on the species level, either by using different classifiers such as maximum likelihood (Wang et al., 2004; Lee and Yeh, 2009) or object-based (Heumann, 2011; Lehmann et al., 2015), or using more information from more spectral bands (Lee and Yeh, 2009), texture (Pu and Cheng, 2015), and pixel spatial location (Lehmann et al., 2015). However, our study was designed to quantify changes in canopy density over time and not shifts in species, and canopy density is found to be highly correlated with vegetation indices such as SR (Green et al., 1998; Kuenzer et al., 2011; Pu and Cheng, 2015). This ensures that our approach is still useful despite the issues presented above. Fourth, we used imagery from different seasons, the aerial photographs were collected in April (2008) and December (2010), the dryer season in the area (Ellis and Bell), and the WV2 image was obtained in June (2014), the wetter season. Mangrove litterfall tends to be higher in the summer and wetter season (0.5 g/0.25 m^2) than in the winter-spring dryer season (0.25 g/0.25 m^2; Ellis and Bell, 2004). This may mean that the density classes for the WV2 image may be affected by a higher litter fall than the aerial photographic images. This would only be problematic if the ranges of density of the classes did not overlap and if the results would indicate a marked decrease in the dense class, which was not the case in our study so we are still confident on the changes between 2010 and 2014. Fifth, we made an adjusted SR to be able to compare classifications based on imagery obtained with the WV2 sensor (2014) and aerial photographs, as the sensors spectral bands have different widths. Sixth, we decided to not use the transition growth type sparse mangrove for our landcover classifications as this vegetation type was not accurately predicted. This made our classification more reliable, but some dwarf vegetation that is transitioning to dense vegetation is now either classified as dwarf or as dense. Further, it is important to notice that the non-RIM and the RIM impoundments have been managed for different time periods. Despite all of these limitations, we think that we addressed them with the best possible solutions, and that our results are representative of the effects of RIM on mangrove vegetation density. Our results suggest that the non-RIM management is close to an equilibrium, and that the RIM-imp is the farthest to such equilibrium but in the right trajectory. It must be noted that there were nine months between the collection date of the WV2 images (June 2014) and the collection of the *in situ* LAI measurements (March 2015), in which changes could have taken place in the *in situ* LAI, but the strong correlations found between the *in situ* LAI and the vegetation indices suggest that such changes are likely negligible.

With the use of high resolution aerial photographs and WV2 image we could map the effects of RIM on mangrove density at the scale of the impoundment. The post-classification change detection showed that over the RIM managed impoundment, the area of dense mangrove increased by 22% between 2008 and 2010, and by 21% between 2010 and 2014; a total of 38% from 2008 to 2014. We interpret the large shift in the cover density of plant communities to be primarily because of a decrease in salinity levels that resulted in increased nitrogen availability and increased growth (Verhoeven et al. 2014). As an indication

of the extent of change that has occurred since implementation of RIM, by 2014 the coverage of dense vegetation in the RIM impoundment was similar to the aerial extent of dense vegetation in the adjacent impoundment that is open to tidal exchange.

5. Conclusion

This study illustrates that the implementation of RIM (rotational impoundment management) in an impounded mangrove has been beneficial for the density of mangrove vegetation on the scale of the impoundment. Our results suggest that RIM is beneficial for the re-establishment of vegetation in areas that were previously bare ground or only covered by patches of herbaceous vegetation. The changes in LAI support earlier findings (Verhoeven et al. 2014) that RIM results in increased growth of already established mangroves. Even with increased cover and higher growth rates the mangrove vegetation in the RIM impoundment has not reached the stature of vegetation in the impoundment that is open to tidal circulation or the non-impounded area. This is the first study that makes a comparison between an impounded mangrove which has RIM implemented and an area that has not been impounded. A reason for the observations that the vegetation in the RIM impoundment is of lower stature (i.e., lower LAI) could be that 5 years is a too short period of time to study the full effects of the implementation of RIM and that a longer time horizon is needed to see a full recovery. Nonetheless, this study has documented that RIM has positive benefits for mangrove growth.

Acknowledgements

This study received funding from the stipend Bottelier and Miquel fund. We would like to thank the staff of the Smithsonian Marine Station at Fort Pierce for their help with the fieldwork, this paper is publication number 1089 of the marine station. We would also like to thank Stuart Korte from the Florida Department of Transportation who provided us the CIR photographs free of charge. We would also like to thank the Laboratory of Geoinformation Science and Remote Sensing from Wageningen University for lending us their ASD field spectrometer, which made the radiometric calibration of the aerial photographs possible.

Appendix A. Supplementary data

Supplementary data related to this article can be found at http://dx.doi.org/10.1016/j.ecss.2018.06.020.

References:

A.S.D., 2002. FieldSpec ® Pro User ' S Guide. pp. 1–136.
Alongi, D.M., 2002. Present State and Future of the World' S Mangrove Forests Present State and Future of the World ' S Mangrove Forests. http://dx.doi.org/10.1017/S0376892902000231.
Alongi, D.M., 2008. Mangrove forests: resilience, protection from tsunamis, and responses to global climate change. Estuar. Coast. Shelf Sci. 76, 1–13. http://dx.doi.org/10.1016/j.ecss.2007.08.024.
Atkinson, M.R., Findlay, G.P., Hope, a B., Pitman, M.G., Saddler, H.D.W., West, K.R., 1967. Salt regulation in the mangroves «Rhizophora mucronata» Lam. and «Aegialitis annulata» R.BR. Aust. J. Biol. Sci. 20, 589–599.
Barbier, E., Hacker, S.D., 2011. The value of estuarine and coastal ecosystem services. Ecol. Monogr 81, 169–193.
Belluco, E., Camuffo, M., Ferrari, S., Modenese, L., Silvestri, S., Marani, A., Marani, M., 2006. Mapping salt-marsh vegetation by multispectral and hyperspectral remote sensing. Remote Sens. Environ 105, 54–67. http://dx.doi.org/10.1016/j.rse.2006.06.006.
Bosire, J.O., Dahdouh-Guebas, F., Walton, M., Crona, B.I., Lewis, R.R., Field, C., Kairo, J.G., Koedam, N., 2008. Functionality of restored mangroves: a review. Aquat. Bot 89, 251–259. http://dx.doi.org/10.1016/j.aquabot.2008.03.010.
Brockmeyer, R.E., Rey, J.R., Virnstein, R.W., Gilmore, R.G., Earnest, L., 1996. Rehabilitation of impounded estuarine wetlands by hydrologic reconnection to the Indian River Lagoon, Florida (USA). Wetl. Ecol. Manag 109, 93–109.
Chmura, G.L., Anisfeld, S.C., Cahoon, D.R., Lynch, J.C., 2003. Global carbon sequestration in tidal, saline wetland soils. Global Biogeochem. Cycles 17, 12. http://dx.doi.org/10.1029/2002gb001917.
Christopherson, J., 2010. USGS Quality Assurance Plan for Digital Aerial Imagery, Certification Report for the Microsoft Vexcel UltraCamD, UltraCamX, UltraCamXp, and UltraCamXp WA Models.
Congalton, R.G., 1991. A review of assessing the accuracy of classifications of remotely sensed data. Remote Sens. Environ 37, 35–46. http://dx.doi.org/10.1016/0034-4257(91)90048-B.
Donato, D.C., Kauffman, J.B., Murdiyarso, D., Kurnianto, S., Stidham, M., Kanninen, M., 2011. Mangroves among the most carbon-rich forests in the tropics. Nat. Geosci 4, 293–297. http://dx.doi.org/10.1038/ngeo1123.
Doughty, C.L., Cavanaugh, K.C., Hall, C.R., Feller, I.C., Chapman, S.K., 2017. Impacts of mangrove encroachment and mosquito impoundment management on coastal protection services. Hydrobiologia 803, 105–120. http://dx.doi.org/10.1007/s10750-017-3225-0.
Duke, N.C., Ball, M.C., Ellison, J.C., 1998. Factors influencing biodiversity and distributional gradients in Mangroves. Glob. Ecol. Biogeogr. Lett. 7, 27. http://dx.doi.org/10.2307/2997695.
Ellis, W.L., Bell, S.S., 2004. Canopy gaps formed by mangrove trimming: an experimental test of impact on litter fall and standing litter stock in Southwest Florida (USA). J. Exp. Mar. Bio. Ecol. 311, 201–222. http://dx.doi.org/10.1016/j.jembe.2004.05.008.
Facchi, A., Baroni, G., Boschetti, M., Gandolfi, C., 2012. Comparing opticaland direct methods for leafarea index determination in a maize crop. J. Agric. Eng 41, 33–40. http://dx.doi.org/10.4081/jae.2010.1.33.
Feller, I.C., Whigham, D.F., McKee, K.L., Lovelock, C.E., 2003. Nitrogen limitation of growth and nutrient dynamics in a disturbed mangrove forest, Indian River Lagoon, Florida. Oecologia 134, 405–414. http://dx.doi.org/10.1007/s00442-002-1117-z.
Feller, I.C., Friess, D.A., Krauss, K.W., Lewis III, R.R., 2017. The state of the world's mangroves in the 21st century under climate change. Hydrobiologia 803, 1–12. http://dx.doi.org/10.1007/s10750-017-3331-z.
Geneletti, D., Gorte, B.G.H., 2003. A method for object-oriented land cover classification combining Landsat TM data and aerial photographs. Int. J. Remote Sens 24, 1273–1286. http://dx.doi.org/10.1080/01431160210144499.
Giri, C., Ochieng, E., Tieszen, L.L., Zhu, Z., Singh, A., Loveland, T., Masek, J., Duke, N., 2011. Status and Distribution of Mangrove Forests of the World Using Earth. pp. 154–159. http://dx.doi.org/10.1111/j.1466-8238.2010.00584.x.
Gonsamo, A., Pellikka, P., 2012. The sensitivity based estimation of leaf area index from spectral vegetation indices. ISPRS J. Photogramm. Remote Sens 70, 15–25.
Green, E.P., Clark, C.D., Mumby, P.J., Edwards, A.J., Ellis, A.C., 1998. Remote sensing techniques for mangrove mapping. Int. J. Remote Sens 19, 935–956. http://dx.doi.org/10.1080/014311698215801.
Hadjimitsis, D.G., Clayton, C.R.I., Retalis, A., 2009. The use of selected pseudo-invariant targets for the application of atmospheric correction in multi-temporal studies using satellite remotely sensed imagery. Int. J. Appl. Earth Obs. Geoinf 11, 192–200. http://dx.doi.org/10.1016/j.jag.2009.01.005.
Hatton, J.C., Couto, A.L., 1992. The effect of coastline changes on mangrove community structure, Portuguese Island, Mozambique. Hydrobiologia 247, 49–57.
Heenkenda, M., Joyce, K., Maier, S., Bartolo, R., 2014. Mangrove species identification: comparing WorldView-2 with aerial photographs. Remote Sens 6, 6064–6088. http://dx.doi.org/10.3390/rs6076064.
Heumann, B.W., 2011a. Satellite remote sensing of mangrove forests: recent advances and future opportunities. Prog. Phys. Geogr 35, 87–108. http://dx.doi.org/10.1177/0309133310385371.
Heumann, B.W., 2011b. An object-based classification of mangroves using a hybrid decision tree-support vector machine approach. Remote Sens 3, 2440–2460. http://dx.doi.org/10.3390/rs3112440.
Honkavaara, E., Arbiol, R., Markelin, L., Martinez, L., Cramer, M., Bovet, S., Chandelier, L., Ilves, R., Klonus, S., Marshal, P., Schläpfer, D., Tabor, M., Thom, C., Veje, N., 2009. Digital airborne photogrammetry—a new tool for quantitative remote Sensing?—A state-of-the-art review on radiometric aspects of digital photogrammetric images. Remote Sens 1, 577–605. http://dx.doi.org/10.3390/rs1030577.
Humphrey, J., 2011. Florida minimum Technical Standards for Projects, Survey & Map Report.
Intergraph, 2009. Digital Mapping Camera System.
Jimenez, J.A., Lugo, A.E.A., Cintron, G., 1985. Tree mortality in mangrove forests. Biotropica 17, 177–185. http://dx.doi.org/10.1016/0198-0254(86)91196-9.
Kovacs, J.M., King, J.M.L., Flores de Santiago, F., Flores-Verdugo, F., 2009. Evaluating the condition of a mangrove forest of the Mexican Pacific based on an estimated leaf area index mapping approach. Environ. Monit. Assess 157, 137–149. http://dx.doi.org/10.1007/s10661-008-0523-z.
Kovacs, J.M., Wang, J., Flores-Verdugo, F., 2005a. Mapping mangrove leaf area index at the species level using IKONOS and LAI-2000 sensors for the Agua Brava Lagoon, Mexican Pacific. Estuar. Coast. Shelf Sci. 62, 377–384. http://dx.doi.org/10.1016/j.ecss.2004.09.027.
Kovacs, J.M., Wang, J., Flores-Verdugo, F., 2005b. Mapping mangrove leaf area index at the species level using IKONOS and LAI-2000 sensors for the Agua Brava Lagoon, Mexican Pacific. Estuar. Coast. Shelf Sci. 62, 377–384. http://dx.doi.org/10.1016/j.ecss.2004.09.027.
Krause, G., Bock, M., Weiers, S., Braun, G., 2004. Mapping land-cover and mangrove structures with remote sensing techniques: a contribution to a synoptic GIS in support of coastal management in North Brazil. Environ. Manage 34, 429–440. http://dx.doi.org/10.1007/s00267-004-0003-3.
Kuenzer, C., Bluemel, A., Gebhardt, S., Quoc, T.V., Dech, S., 2011. Remote Sensing of Mangrove Ecosystems: a Review, Remote Sensing. http://dx.doi.org/10.3390/rs3050878.
Laanbroek, H.J., Keijzer, R.M., Verhoeven, J.T a, Whigham, D.F., 2012. The distribution of ammonia-oxidizing betaproteobacteria in stands of black mangroves (Avicennia

germinans). Front. Microbiol. 3, 153. http://dx.doi.org/10.3389/fmicb.2012.00153.
Laben, C., Brower, B., 2000. Process for enhancing the spatial resolution of multispectral imagery using pan-sharpening. United States Pat 6 (11), 875.
Landis, J.R., Koch, G., 1977. An application of hierarchical kappa-type statistics in the assessment of majority agreement among multiple observers. Int. Biometric Soc. 33, 363–374.
Lee, T.M., Yeh, H.C., 2009. Applying remote sensing techniques to monitor shifting wetland vegetation: a case study of Danshui River estuary mangrove communities. Taiwan. Ecol. Eng 35, 487–496. http://dx.doi.org/10.1016/j.ecoleng.2008.01.007.
Lehmann, J., Nieberding, F., Prinz, T., Knoth, C., 2015. Analysis of unmanned aerial system-based CIR images in forestry—a new perspective to monitor pest infestation levels. Forests 6, 594–612. http://dx.doi.org/10.3390/f6030594.
Machado, J., Reich, P.B., 1999. Evaluation of Several Measures of Canopy Openness as Predictors of Photosynthetic Photon Flux Density in Deeply Shaded conifer-dominated forest Understory 1444. pp. 1438–1444.
Manakos, I., Manevski, K., Kalaitzidis, C., Edler, D., 2011. Comparison between FLAASH and ATCOR atmospheric correction modules on the basis of Worldview-2 imagery and in situ spectroradiometric measurements. EARSeL 7th SIG-Imaging Spectrosc. Work 11.
Padwick, C., Deskevich, M., Pacifici, F., Smallwood, S., 2010. Worldview-2 pan-sharpening.
Pu, R., Cheng, J., 2015a. Mapping forest leaf area index using reflectance and textural information derived from WorldView-2 imagery in a mixed natural forest area in Florida, US. Int. J. Appl. Earth Obs. Geoinf 42, 11–23. http://dx.doi.org/10.1016/j.jag.2015.05.004.
Pu, R., Cheng, J., 2015b. Mapping forest leaf area index using reflectance and textural information derived from WorldView-2 imagery in a mixed natural forest area in Florida, US. Int. J. Appl. Earth Obs. Geoinf 42, 11–23. http://dx.doi.org/10.1016/j.jag.2015.05.004.
Pu, R., Landry, S., 2012. A comparative analysis of high spatial resolution IKONOS and WorldView-2 imagery for mapping urban tree species. Remote Sens. Environ 124, 516–533. http://dx.doi.org/10.1016/j.rse.2012.06.011.
Qi, J., Chehbouni, a., Huete, a. R., Kerr, Y.H., Sorooshian, S., 1994. A modified soil adjusted vegetation index. Remote Sens. Environ 48, 119–126. http://dx.doi.org/10.1016/0034-4257(94)90134-1.
Ramsey, E.W., Jensen, J.R., 1996. Remote sensing of mangrove wetlands: relating canopy spectra to site-specific data. Photogramm. Eng. Remote Sensing 62, 939–948.
Rey, J., O'Connell, S., Carlson, D., Brockmeyer, R., 2009. Characteristics of mangrove swamps managed for mosquito control in eastern Florida, USA: a re-examination. Mar. Ecol. Prog. Ser 389, 295–300. http://dx.doi.org/10.3354/meps08256.
Rey, J.R., Crossman, R.a., Kain, T.R., 1990. Vegetation dynamics in impounded marshes along the Indian River lagoon, Florida, USA. Environ. Manage 14, 397–409. http://dx.doi.org/10.1007/BF02394208.
Rey, J.R., Walton, W.E., Wolfe, R.J., Connelly, C.R., O'Connell, S.M., Berg, J., Sakolsky-Hoopes, G.E., Laderman, A.D., 2012. North American wetlands and mosquito control. Int. J. Environ. Res. Public Health 9, 4537–4605. http://dx.doi.org/10.3390/ijerph9124537.
Rodriguez, W., Feller, I.C., 2004. Mangrove landscape characterization and change in Twin Cays, Belize using aerial photography and IKONOS satellite data. Atoll Res. Bull 1–22. http://dx.doi.org/10.1007/s13398-014-0173-7.2.
Stringer, C.E., Rains, M.C., Kruse, S., Whigham, D., 2010. Controls on water levels and salinity in a barrier island mangrove, Indian River lagoon, Florida. Wetlands 30, 725–734. http://dx.doi.org/10.1007/s13157-010-0072-4.
Tomlinson, P.B., 1986. The Botany of Mangroves. Cambridge Tropical Biology Series. Cambridge University Press.
Updike, T., Comp, C., 2010. Radiometric Use of WorldView-2 Imagery Technical Note 1 WorldView-2 Instrument Description. pp. 1–17.
Vega-Rodríguez, M., 2008. Estimating primary productivity of red mangroves in southwestern Puerto Rico from remote sensing and field measurements. Mar. Sci. Master 81.
Verhoeven, J.T.a, Laanbroek, H.J., Rains, M.C., Whigham, D.F., 2014. Effects of increased summer flooding on nitrogen dynamics in impounded mangroves. J. Environ. Manage 139, 217–226. http://dx.doi.org/10.1016/j.jenvman.2014.02.035.
Vogt, J., Skóra, A., Feller, I.C., Piou, C., Coldren, G., Berger, U., 2012. Investigating the role of impoundment and forest structure on the resistance and resilience of mangrove forests to hurricanes. Aquat. Bot. 97, 24–29. http://dx.doi.org/10.1016/j.aquabot.2011.10.006.
Wang, L., Sousa, W.P., Gong, P., Biging, G.S., 2004. Comparison of IKONOS and QuickBird images for mapping mangrove species on the Caribbean coast of Panama. Remote Sens. Environ 91, 432–440. http://dx.doi.org/10.1016/j.rse.2004.04.005.
Wilhelm, W.W., Ruwe, K., Schlemmer, M.R., 2000. Comparison of three leaf area index meters in a corn canopy. Crop Sci. 40, 1179–1183. http://dx.doi.org/10.2135/cropsci2000.4041179x.
Zhao, D., Huang, L., Li, J., Qi, J., 2007. A Comparative Analysis of Broadband and Narrowband Derived Vegetation Indices in Predicting LAI and CCD of a Cotton Canopy 62. pp. 25–33. http://dx.doi.org/10.1016/j.isprsjprs.2007.01.003.